INL/EXT-21-64432
Revision 0

Predictive Data Analytics Framework Using Advanced Test Reactor Acoustic Data

September 2021

Vivek Agarwal, James A. Smith
Nuclear Science and Technology Directorate

Veryl C. Kirkpatrick
Advanced Test Reactor

Idaho National Laboratory

INL is a U.S. Department of Energy National Laboratory
operated by Battelle Energy Alliance, LLC

INL/EXT-21-64432
Revision 0

Predictive Data Analytics Framework Using Advanced Test Reactor Acoustic Data

Vivek Agarwal, James A. Smith
Nuclear Science and Technology Directorate
Veryl C. Kirkpatrick
Advanced Test Reactor

September 2021

Idaho National Laboratory
Originating Organization
Idaho Falls, Idaho 83415

http://www.inl.gov

Prepared for the
U.S. Department of Energy
Office of Nuclear Energy
Under DOE Idaho Operations Office
Contract DE-AC07-05ID14517

Page intentionally left blank

ABSTRACT

Although a nuclear reactor is a hostile environment for sensing and electrical communications, the reactor core is amenable to acoustic communication. An acoustic measurement infrastructure (AMI) has been installed at the Advanced Test Reactor (ATR) nozzle trench area to record acoustic signals that have the ability to capture different operating regimes of the reactor. This AMI includes ATR in-pile structural components, coolant, acoustic receivers, and primary coolant pumps as signal sources, a data acquisition system, and signal-processing algorithms enabling real-time monitoring.

This report will discuss development of a recursive Short Time Fast Fourier Transform (STFFT) approach to process acoustic signals. The recursive STFFT is then applied to the data obtained from the ATR brush experiment to understand the vibration levels and to develop spectrograms for different operating regimes. The combination of primary coolant pumps for normal and power axial locator mechanisms of ATR are different and generate unique signatures. These acoustic signatures were used to develop machine learning approaches to automatically classify different operating regimes. This lays the foundation for a predictive analytic framework that can be leveraged by ATR to optimize their operations and maintenance.

The path forward involves continued engagement with ATR and expanded implementation of the AMI and predictive framework at ATR and other facilities within Idaho National Laboratory and at other experimental reactors.

ACKNOWLEDGEMENTS

This report was made possible through funding by the U.S. Department of Energy's Nuclear Energy Enabling Technologies Program. We are grateful to Melissa Bates and Daniel Nichols at the U.S. Department of Energy as well as Pattrick Calderoni at Idaho National Laboratory for championing this effort. We thank Rebecca N. Ritter and Nikki M. Peterson at Idaho National Laboratory for technical editing and formatting of the document.

Page intentionally left blank

CONTENTS

FIGURES

TABLES

Page intentionally left blank

ACRONYMS

AMI	Acoustic Measurement Infrastructure
ASI	Advanced Sensors and Instrumentation
ATR	Advanced Test Reactor
FFT	Fast Fourier Transform
HSIS	hydraulic shuttle irradiation system
LDA	Linear Discriminant Analysis
NN	neural networks
PALM	Power Axial Locator Mechanism
PCP	primary coolant pump
STFFT	Short-term Fast Fourier Transform
SV	support vector
SVM	support vector machine

Page intentionally left blank

Predictive Data Analytics Framework Using Advanced Test Reactor Acoustic Data

1. INTRODUCTION

Although a nuclear reactor is a hostile environment for sensing and electrical communications, the reactor core is amenable to acoustic telemetry. Acoustic-based sensor systems are of interest for several reactor programs to take advantage of the acoustic transmission properties of the core. Fuel Cycle Research and Development and the Advanced Reactor Technologies programs have collaborated to install acoustic/vibration sensors on and around the Advanced Test Reactor (ATR) [1] containment vessel. Installation of the acoustic/vibration receivers represents the first step in developing an acoustic communication infrastructure. The proposed acoustic measurement infrastructure (AMI) will accommodate sensor design and signal-processing tools for telemetry systems that use acoustic-based sensors, such as thermoacoustics [2–4] and vibro-acoustics [5]. The acoustic infrastructure will also provide an excellent opportunity to develop diagnostic and predictive capabilities for ATR operations.

The objective of this research is to develop a predictive data analytics framework using ATR Acoustic Data. This report will discuss the initial signal-processing techniques used in the ATR acoustic telemetry infrastructure and the resulting data. The long-term strategic goal is to establish a predictive data analytics framework for ATR and then adapt the framework for the Transient Reactor Test Facility [6]. This type of acoustic infrastructure and predictive framework would be the first of a kind for nuclear applications. Once fully in place, the acoustic telemetry based predictive framework would also enable reactors to be operated more efficiently by using the diagnostic/prognostic health monitoring and predictive maintenance algorithms developed during this project.

1.1 Predictive Maintenance Framework Motivation

The fundamental premise behind this work is the belief that listening to a reactor's intrinsic (normal reactor operation) and extrinsic acoustic sources (active sensors) will allow for a Predictive Data Analytics Framework when coupled with advanced data analytic algorithms. Early detection of structural failures, pump/vane degradation, and other diverse faults inside reactors are possible with proper sensing and data processing/classification techniques. Multiple signals from several nonintrusive acoustic receivers provide an ability to assess operating conditions with no impact on reactor safety or control systems.

This predictive data analytics framework is novel as it relies on data transmitted wirelessly from inside to outside of the reactor; and it is also practical as it will provide the unique ability to perform nonintrusive in reactor measurements. This wireless transmission refers to the transmission of sound via fluids, mechanical structures, pipes, and conduits. The acoustic signals are received by acoustic/vibrational receivers located on the exterior of the pressure vessel or on vessel piping. The transmission of signals will allow users and experimenters to access raw data, process the data, and extract information from the signal while the reactor is operating.

With the vibrational baseline and active monitoring of the reactor, it will be possible to prevent component failures in experiments such as what happened in ATR Full Size In Flux Trap Position-6 MKII. A non-fueled component (the bottom plate) of the first fuel plate frame assembly separated from the rail sides in the ATR. The separation of this component was caused by flow induced vibrations, where vortex shedding frequencies were resonant with a natural frequency of the bottom plate component. As a result, amplification and fracture occurred and led to separation from the assembly [7]. It would have been possible to detect the vortex-induced vibrations had a vibrational baseline and active vibration monitoring been in place with the appropriate data analytics framework. The experiment could then have been removed from the ATR before the failure of the component.

1.2 Report Layout

The rest of the report is organized as follows:

- Section 2 describes the AMI used to collect real-time acoustic data and the recursive application of the Short Time Fast Fourier Transform (STFFT) used to process the data
- Section 3 details the acoustic data analysis of real-time and processed data collected using AMI
- Section 4 describes the acoustic spectrograms generated during normal and power axial locator mechanism (PALM) cycle of ATR operation
- Section 5 lays down the predictive data analysis framework showing the application of support vector machine (SVM) and linear discriminant analysis (LDA) approaches to classify the data based on ATR operating conditions
- Section 6 summarizes the results and describes path forward.

2. ACOUSTIC MEASUREMENT INFRASTRUCTURE

The current implementation of the AMI includes ATR in-pile structural components, coolant, acoustic receivers, primary coolant pumps (PCPs) as signal sources, a data acquisition system, and signal-processing algorithms that enables real-time measurement.

2.1 Acoustic Receivers and their Locations

Eight accelerometers [8] were placed on the circumference of the ATR pressure vessel in June 2015. All the accelerometers—which have a sensitivity of 100mV/g and operating frequency of 1 to 17 kHz—were installed in the nozzle trench area. The general location of the nozzle trench area in ATR is shown in Figure 1. The nozzle trench area allows for convenient access to the upper portion of the ATR pressure vessel. The average radiation level in the ATR nozzle trench area during reactor operation is 0.165 R/h. Thus far, the accumulated absorbed radiation has had no impact on the installed piezoelectric accelerometers and other electronics. The installed accelerometers to date are functioning as expected; they have performed reliably for thirteen regular ATR cycles and five PALM cycles. The accelerometers are placed at different locations on the pressure vessel and access flanges at irregular intervals covering approximately three quarters of the pressure vessel circumference. The accelerometers are connected to a National Instruments Compact Data Acquisition System [9] and processing system which forms the AMI [9–11].

Five of the eight accelerometer locations in the ATR nozzle trench area are shown in Figure 2. The accelerometers are placed on pressure vessel on different flanges and on the piping for the hydraulic shuttle irradiation system (HSIS). The channel numbers are the analog to the digital converter signal channels in the data acquisition board.

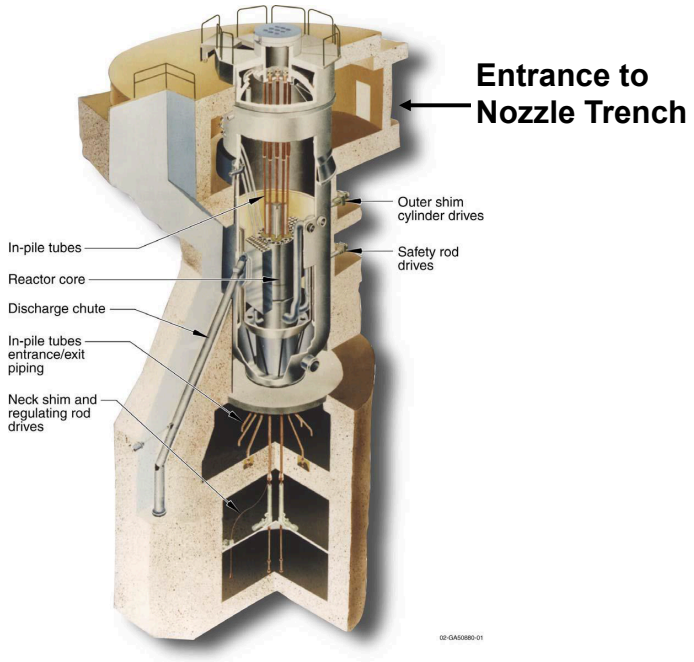

Figure 1. A schematic of ATR showing the location of the nozzle trench area.

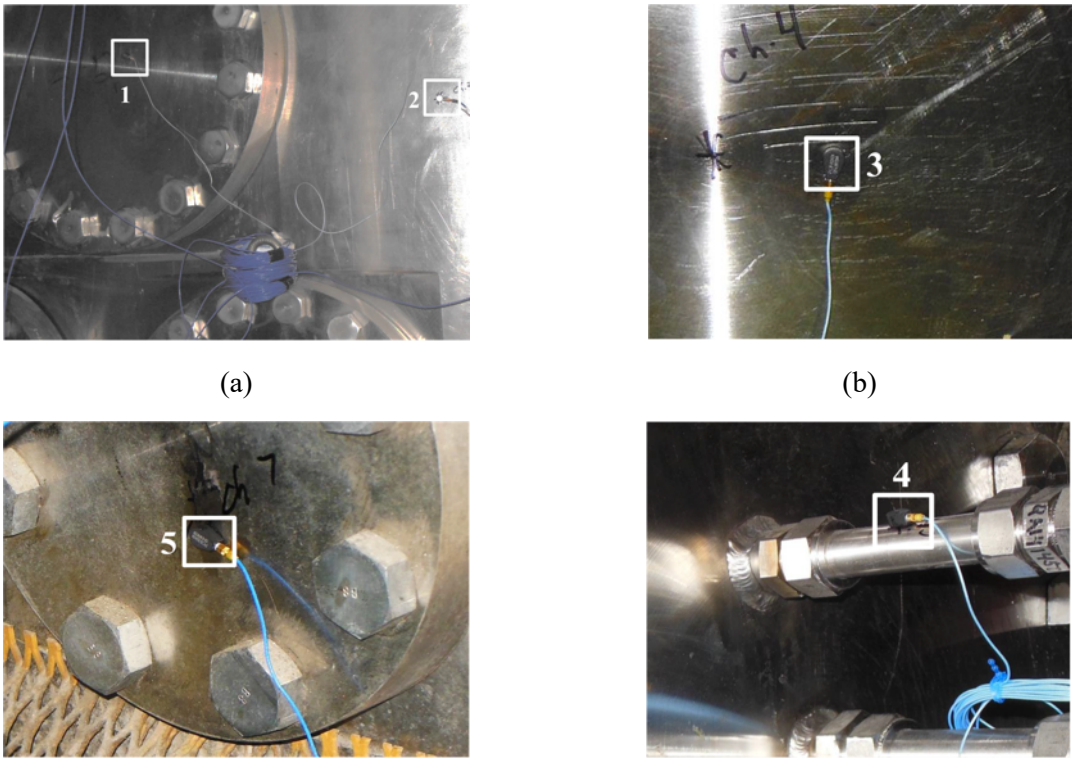

(a) (b)

(c) (d)

Figure 2. Piezoelectric accelerometers (acoustic receivers) installed in the nozzle trench area of the ATR. (a) Receiver Location 1 corresponds to the L2 flange and Receiver Location 2 corresponds to the pressure vessel, (b) Receiver Location 3 corresponds to the L7 flange, (c) Receiver Location 4 corresponds to the HSIS, and (d) Receiver Location 5 corresponds to the C13 flange.

2.2 Recursive Use of the Short Time Fast Fourier Transform

The raw real-time data has been processed using a STFFT algorithm [12–27]. The AMI acquires and processes sensor data in real-time for process monitoring, diagnostics, and prognostics. AMI continuously captures analog signal data from the acoustic sensors (i.e., accelerometers) and digitizes the signals before saving either the raw signal or the processed STFFT [28] signal but not both. The STFFT is composed from the repetitive use of a shifted time windowed Fast Fourier Transform (FFT) over the continuous data set. The FFT data contains multiple frequencies of interest. To capture specific harmonics of interest, one or more frequency bandwidths are chosen to be monitored within the sequenced time-frequency spectrum. The maximum amplitude, frequency at the maximum amplitude and corresponding phase for the selected frequency harmonics, are then sequentially written to a file for additional processing.

During real-time analysis, a FFT is applied to the digitized acoustic data. From the resulting frequency spectra, frequency bandwidths of interest are chosen. Once the frequency bandwidths are selected, a STFFT is performed on the digitized data using a sliding time window, T. From the STFFT data, one or more frequency bandwidths of interest may be selected to monitor over time. Each selected frequency bandwidth produces a corresponding maximum amplitude, frequency, and phase sequenced in time. The STFFT involves a repetitive step to generate sequential output data by shifting T by a set time increment generally less than T. By applying the FFT on each time shifted window, the STFFT processes the data in a time sequenced manner. The maximum amplitude and corresponding frequency and phase within the selected frequency bandwidths are monitored to determine the dynamic changes in the industrial process of interest. Selection of the sliding time window size, T, is based on the desired frequency resolution and the signal's frequency stability within the process being monitored. A noisy or shifting harmonic frequency is counter to frequency accuracy. A generic rule of thumb for choosing T is the following. T should be approximately 10 times the time period of the frequency harmonic of interest (e.g., the time window contains at least 10 frequency cycles). From this starting point, the time window size can then be adjusted.

If the process being monitored is expected to be very dynamic and have a fast-changing rate, a smaller time window may be more appropriate. If a stable signal is expected, a longer time window may be more appropriate. As a result, the time window length should be adjusted accordingly and is dependent on the process being monitored. One needs to note that a large time window increases frequency resolution but decreases time resolution. A shorter time window increases time resolution but decreases frequency resolution. Thus, the choice of the time window length is a compromise between time and frequency resolution.

If the STFFT output varies cyclically, it may be appropriate to recursively apply the STFFT to previous STFFT output: amplitude, frequency, and phase. The resulting data from recursive use of the STFFT can then be used to detect trends and/or deviations. The STFFT can be recursively applied as many times as necessary. The signal type (frequency, amplitude, or phase) does not need to remain constant. For example, the raw sensor data can be processed by the STFFT. The amplitude from the pump harmonic can be seen to cyclically vary due to modulation (interference from the two-pump operation). The STFFT can be performed on the time varying amplitudes from the pump harmonic. The resulting STFFT processing provides the center frequency, amplitude, and phase of the modulation. If the resulting center frequency varies cyclically, the STFFT can be recursively applied to the center frequency data to quantify the changes in the modulation frequencies.

For ATR operations, either two (during normal operation) or three (during the PALM cycle) PCPs are operated. Each PCP generates a nominal vane frequency around 148.3 Hz as shown in Figure 3. The 148.3 Hz frequency component is generated by the rotating vanes within each pump. Figure 3 is a FFT at a single instant of time that shows there are other frequency components that could be of interest. Note not every sensor location contains the fundamental pump frequency as indicated by the C-13 flange. The second harmonic, 296.3 Hz of the fundamental pump frequency, is also of interest. The center frequencies

from the operating pumps are different by fractions of Hz and can vary with time. The frequency differences between the two or three slightly different PCP frequencies cause an amplitude modulation of the 148.3 Hz fundamental frequency. Thus, the varying amplitude data from the first STFFT can be recursively input into the STFFT process and provide information and insight on the behavior of the modulating pump frequencies as shown in Figure 4. The processing and identifying of unique process signatures generated by the STFFT are presented in this report.

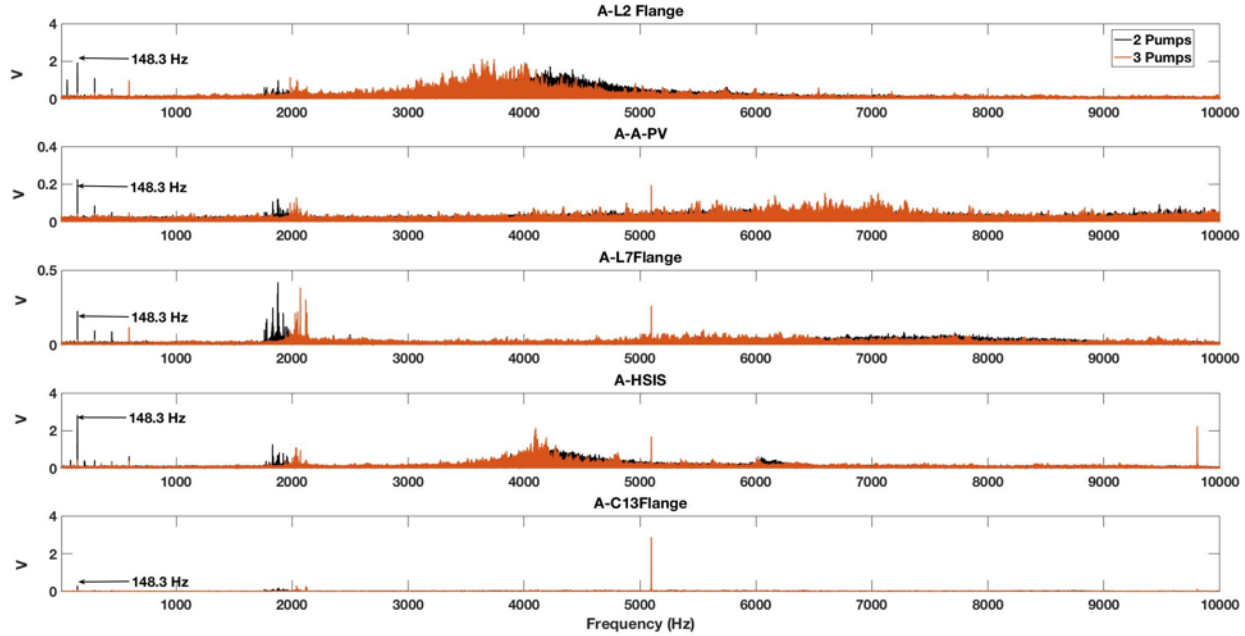

Figure 3. Frequency spectrum of acoustic signals recorded by five piezoelectric sensors installed in the ATR nozzle trench area. The pump vane frequency (at 148.3 Hz) and its harmonics are clearly observed in the frequency spectrum for both 2 and 3 pumps combinations.

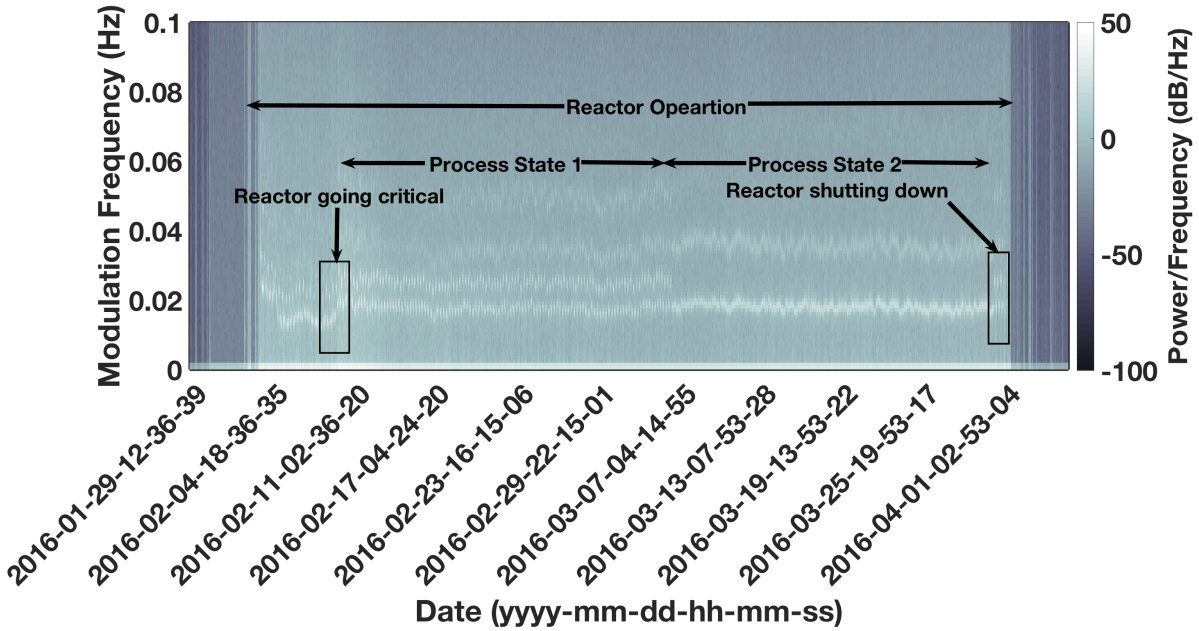

Figure 4. Acoustic baseline signature of ATR collected during reactor operation using the AMI. The plot shows several reactor states: going critical, Process States 1 and 2, and the reactor shutting down.

3. ACOUSTIC DATA ANALYSIS

3.1 Real-Time Acoustic Signal Analysis

On March 3, 2019, a neutron flux sensor called the brush sensor was reporting abnormally high dynamic readings. The brush sensor detects motion within the reactor as the neutron flux reading varies inversely as the square of the distance from the radiation source. ATR operations were concerned there may be a vibration issue. The reactor was shut down due to this vibration concern.

The acoustic/vibration data were collected using the AMI when the plant restarted. Historically, the acoustic sensor data has been processed in real time by AMI. The AMI system would perform a STFFT on the selected sensor channels and for selected frequency windows. Since the data was processed in real time via the STFFT, the amount of data to store is significantly less than storing the raw data. Because of the possible vibration concern and the unfamiliarity of the effects on the sensors, it was decided to save and store all the raw data. This was not a trivial task as 15 days of data consists of 29,000 files with each file of 17.7 MB in size, resulting in a total of 0.53 TB of data.

An automated STFFT program was developed to process the raw data and store the output for later display and processing. The automated STFFT processing program was developed in the following sequence within the MATLAB environment. An STFFT algorithm was developed from the beginning since the amount of raw data caused a memory error in the existing MATLAB algorithm. The custom STFFT algorithm was tested using simulated signals. Then the developed routines were used to automatically read in the raw datafiles, process the data, output the resulting data to files, and display the results. The steps taken to produce the final results are discussed in the following sub-section.

3.1.1 Validating the large data STFFT processing algorithm

As mentioned earlier, the amount of raw data caused a memory error in the existing STFFT routine in MATLAB. A specialized STFFT algorithm was developed using MATLAB's FFT algorithms. To validate the custom designed STFFT and proper selection of useful frequency bandwidths, numeric data sets were generated and processed. The results are shown in Figure 5. Each plot, Figure 5(a)–Figure 5(d), is a different trial run. The center frequency of the selected bandwidth (e.g. 148 Hz for Figure 5(a)) is given at the top of each plot. The frequencies of the numerically generated data are given within the plots. The STFFT algorithm can accurately track the numerically generated frequencies with time.

The STFFT algorithm was then tested on raw data from the ATR AMI. The results are shown in Figure 6. As shown in Figure 6, the STFFT has locked onto the ATR Pump harmonic at ≈ 148.5 Hz. Both pumps produce a frequency close to 148.5 Hz and the two frequencies are combined and interfere. The combined 148.5 Hz harmonic is being frequency modulated by the two primary ATR pumps that produce two interfering frequencies.

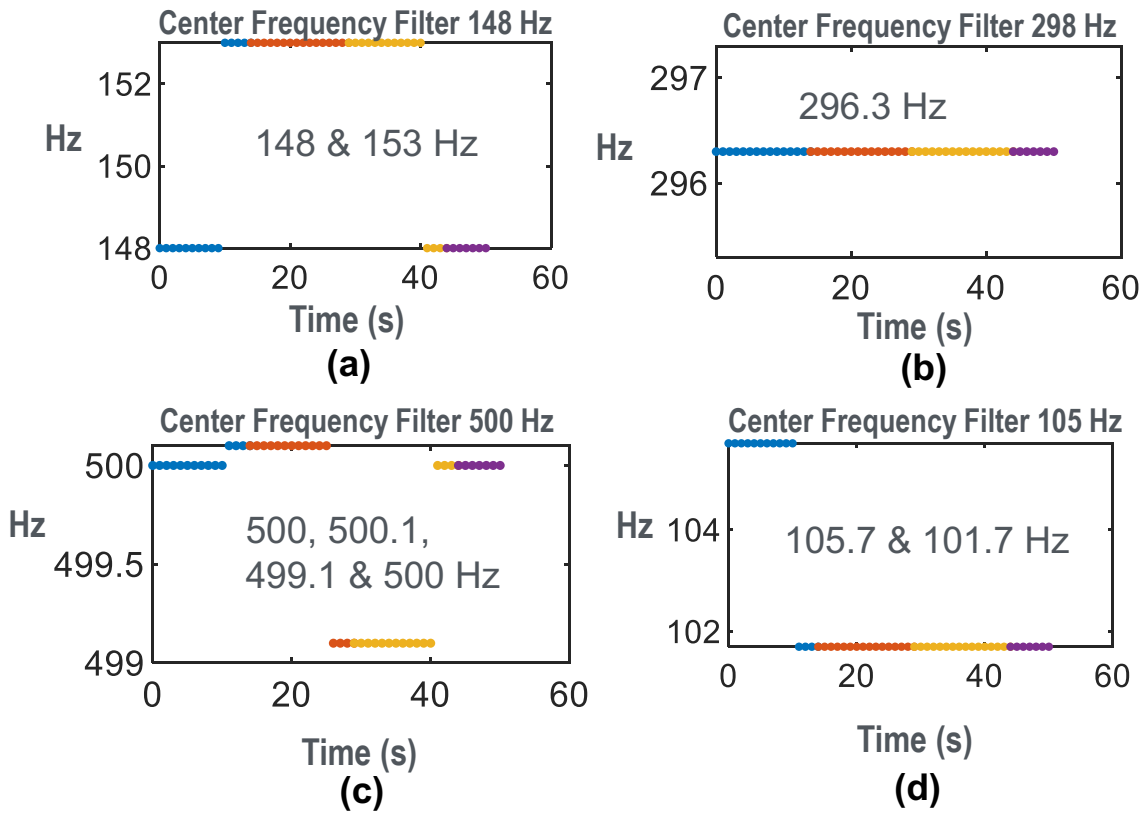

Figure 5. The input data was numerically generated to confirm the developed STFFT processing technique selects the frequency with the maximum amplitude. The numerically generated frequencies are listed within each graph. (a) Center frequencies at 148 and 153 Hz, (b) Constant center frequency at 296.3 Hz, (c) Center frequencies at 500, 500.1, 499.1 and 500 Hz, (d) Center frequencies at 105.7 and 101.7 Hz.

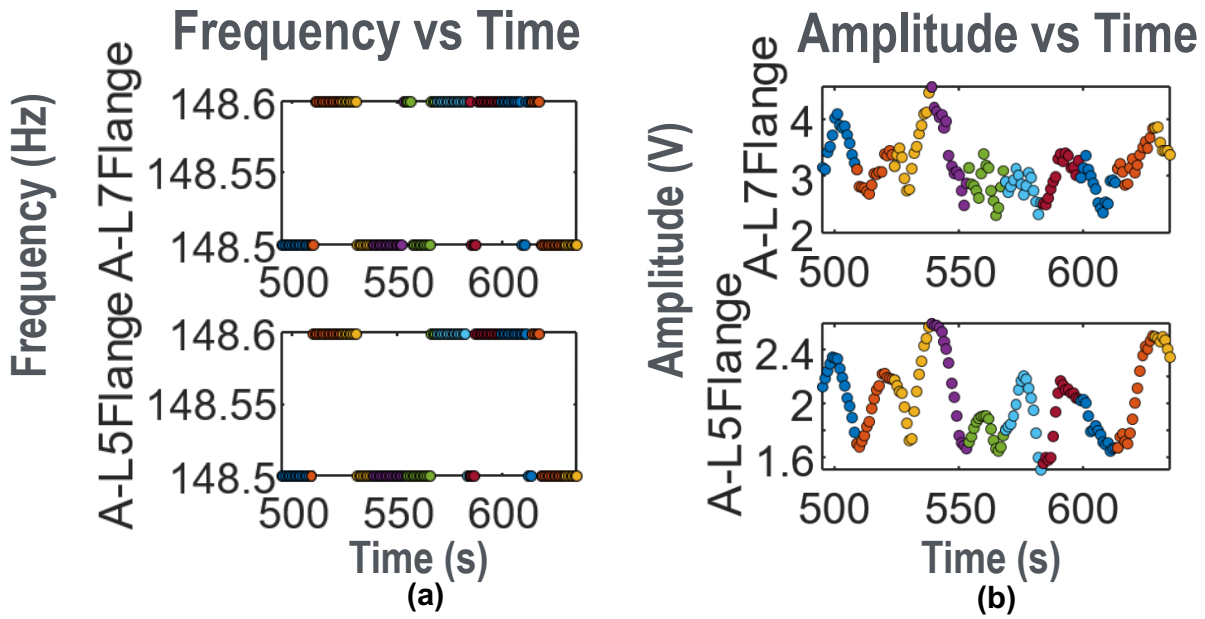

Figure 6. STFFT figures showing (a) STFFT has locked onto the ATR Pump frequency ≈ 148.5 Hz. (b) The 148.5 Hz harmonic is being frequency modulated by the two primary ATR pumps that interfere.

Once the different computational components of the STFFT analysis were tested, the next step was to put together all of the components and validate the results against known ATR process changes. Raw acoustic data during the May 2019 brush investigation were used to validate the complete STFFT analysis routines. Figure 7 shows the partial results of processing 15 days of acoustic data and displaying the salient time period. When the primary pump harmonic is present, the harmonic is ≈ 148.5 Hz. The signal tends to change based on actions taken by the plant as noted in the figure. The pump operational frequency remains stable, but the measured amplitude changes as shown by the red trace in Figure 7. The amplitude signal is frequency and amplitude modulated as can be seen from 12:30 to 14:50. The modulation goes away during single pump operation. A more detailed analysis will be given later in the report.

The recently developed STFFT processing application has been verified and validated. The computational portion of the code was verified by using numerically simulated data. The complete STFFT application was validated by processing ATR brush experimentation data and comparing the timing of the process moves with the timing within the STFFT processed data.

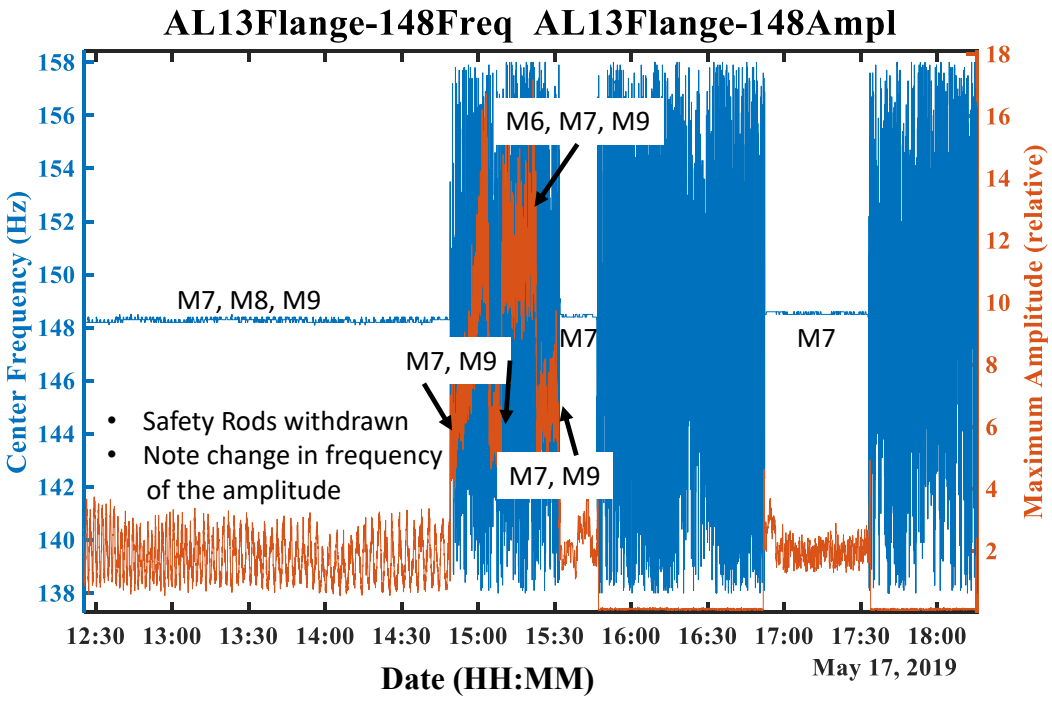

Figure 7. The STFFT processing application can process and display a large amount of acoustic data. The validity of the resulting processed data has been confirmed by ATR process moves as recorded in the electronic logbook.

3.2 Processed Acoustic Data Analysis

The virtual channels resulting from the first pass STFFT processing are shown in Table 1 for the data taken in May 2019. Remember each virtual channel has the following time sequenced data associated with it: maximum amplitude, frequency, and phase. For the purposes of this report, the focus will be on virtual channels generated from the fundamental frequency component near 148.3 Hz. This pump frequency component is created by the PCP. Multiple pumps will produce pump frequency components that will interfere and cause noticeable amplitude modulation in the STFFT generated amplitude data. This phenomenon will prove to be useful for diagnostic and prognostic algorithms. First, the resulting data from the first STFFT will be discussed.

Frequency and amplitude data obtained from the first STFFT provides operational information about the ATR reactor as shown in Figure 8. When there are no pumps running as indicated by the near zero magnitudes in the graph, the STFFT cannot lock in on a pump harmonic because the pumps are not generating vibrations. Once the pumps turn on, the resulting pump harmonic can be tracked. The pump frequency can vary somewhat depending on the state of the reactor. The pumps can also generate higher order harmonics. In general, when the pumps are operating normally, only the fundamental (≈198 Hz) and second order frequencies (≈296 Hz) have enough energy to be noticed above the noise. If the pump is in an abnormal condition such as having a seized bearing, it would be expected stronger higher order harmonics would be generated. Both the frequency and amplitude plots indicate changes in reactor operations and the stability of the reactor process conditions as shown in Figure 8.

Table 1. The list of possible virtual channels produced by the STFFT process is shown. The virtual channels are derived from the raw acoustic data coming from the corresponding Data Acquisition (DAQ) channel.

Virtual Channel	DAQ Channel	Target Frequency (Hz)	Bandwidth (Hz)
A-A-PV_148	A-A-PV	148	10
A-A-PV_298	A-A-PV	298	10
A-A-PV_500	A-A-PV	500	10
A-A-PV_105	A-A-PV	105	10
A-L7Flange_148	A-L7Flange	148	10
A-L7Flange_298	A-L7Flange	298	10
A-L7Flange_500	A-L7Flange	500	10
A-L7Flange_105	A-L7Flange	105	10
A-L5Flange_148	A-L5Flange	148	10
A-L5Flange_298	A-L5Flange	298	10
A-L5Flange_500	A-L5Flange	500	10
A-L5Flange_105	A-L5Flange	105	10
A-HSIS_148	A-HSIS	148	10
A-HSIS_298	A-HSIS	298	10
A-HSIS_500	A-HSIS	500	10
A-HSIS_105	A-HSIS	105	10
A-C13Flange_148	A-C13Flange	148	10
A-C13Flange_298	A-C13Flange	298	10
A-C13Flange_500	A-C13Flange	500	10
A-C13Flange_105	A-C13Flange	105	10
A-L13Flange_148	A-L13Flange	148	10
A-L13Flange_298	A-L13Flange	298	10
A-L13Flange_500	A-L13Flange	500	10
A-L13Flange_105	A-L13Flange	105	10

The information displayed in Figure 8 is useful when only one pump is running. One can baseline the nominal pump frequency and vibration amplitude level for each pump to help understand deviations. As shown in Figure 8, differences can be seen between the individual pumps as well as between the same pump at different running times. It is difficult to determine the causes of the variations as the reactor

operating conditions are dynamic. When multiple pumps are running, additional processing is necessary to monitor operation changes as well as determine the state of the pumps' health. Multiple pumps produce pump frequencies that are closely spaced and difficult to separate. Because the frequencies are closely spaced, they interfere and cause frequency modulation of the pump frequency's amplitude signal. The frequency modulation of the interfering pump frequencies' amplitude contains useful information about the status of the plant's operational state and the health of the pumps.

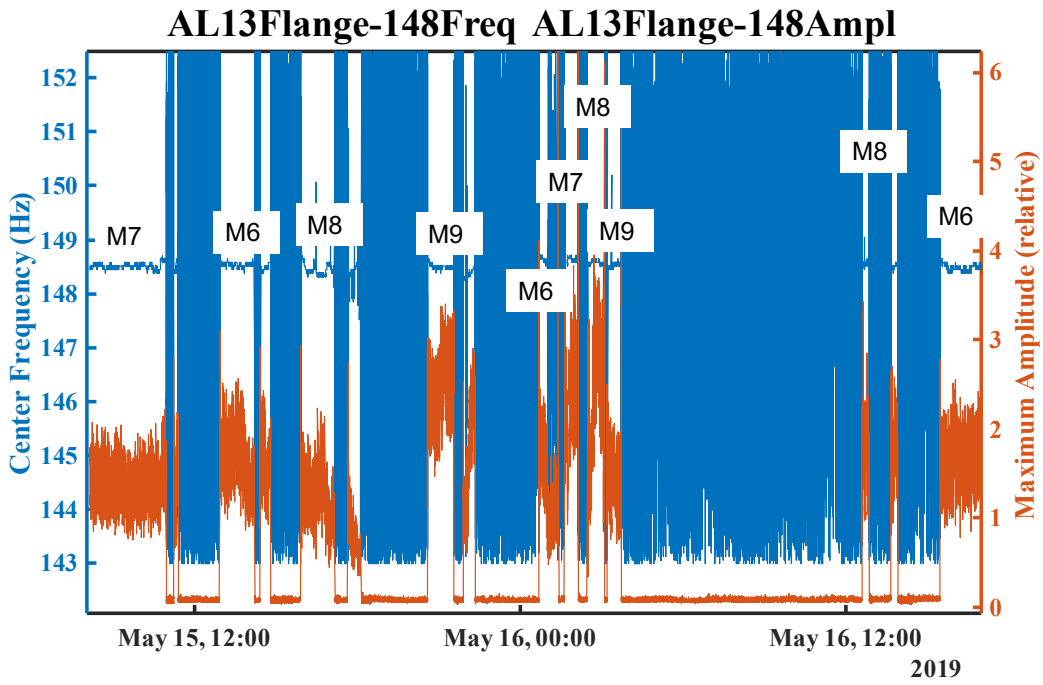

Figure 8. Graph displaying the ATR operation information contained within the frequency and amplitude data from the first STFFT iteration.

As mentioned before, the amplitude data generated from a selected frequency component can be frequency and amplitude modulated as shown in Figure 7. A processing step that recursively uses the STFFT to process the time sequenced amplitude data that has been generated from the first pass STFFT is added. The first pass STFFT processes the raw acoustic data. Then the recursive use of the STFFT on the amplitude data is used to emphasize the changes in frequency modulation of that data, these can be caused by state changes in ATR operations or by changes in pump health.

When there are multiple pumps in operation, the additional STFFT iteration provides unique data and insight into the operational state of the reactor and the health of the pumps. An example of the resulting frequency spectrogram from recursive use of the STFFT is shown in Figure 9. This figure provides interesting insight. The vertical bands are constructed from wideband noise contrasted against the dark blue background in the figure. The pumps provide wideband noise within this spectrogram. Some of the really thin vertical bands on the right side are from the reactor being serviced while in outage.

The features of interest are centered around May 17 at 08:09 . On May 16 around 20:09, ATR operations started cycling through the pumps by turning pumps on and off and, at times, running multiple pumps. The cycling of each of the four pumps lasted approximately 15 to 30 minutes. Figure 9 shows this as the large vertical band starting around 20:09 on May 16 and ending on 23:01. There were no significant indications of a change to multiple pumps running prior to 23:01 on May 16. By 23:01 three pumps, M7, M8 and M9, were running, changing the characteristics of the spectrogram significantly. A nominally horizontal red line appears just above 0.01 Hz. This horizontal line indicates interference between three-pump frequencies close to 148.3 Hz. When the raw data is processed by the first STFFT, the resulting pump frequency amplitudes are cyclically modulated. Figure 7 shows the frequency modulation of the pump frequency's amplitude. This creates a cyclic signal from the amplitude data. Note in Figure 9, the modulation started out just above 0.01 Hz. There was a slight drop in the modulation frequency, and then, the modulation frequency held steady at 0.01 Hz until ATR started to turn the pumps off. The securing of the pumps is indicated by the modulation signal linearly dropping toward 0 Hz. The last pump, M7 was secured at 15:55. At 17:00 on May 17th, the plant tried running M7 for 40 minutes which is displayed as the vertical band right after the three-pump operation. Single pump operation does not produce any modulation features from the recursive use of the STFFT because there is no interference between multiple pumps and thus no modulation.

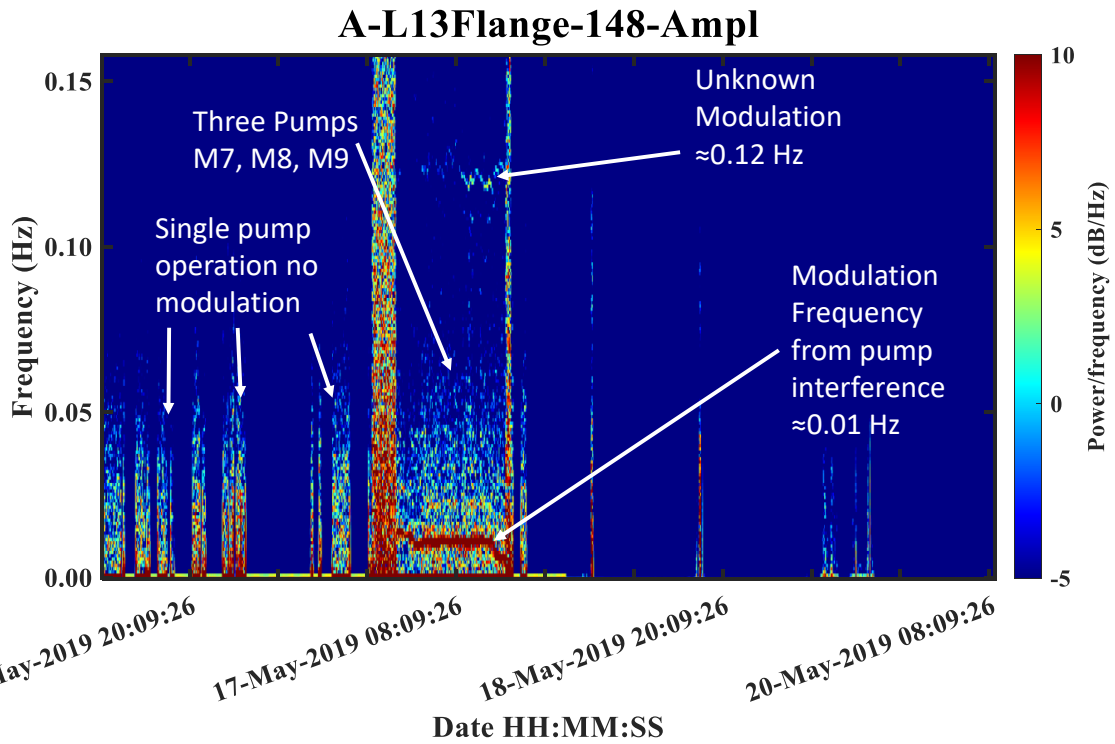

Figure 9. The recursive use of the STFFT generates data that is directly related to the signal interferences caused by multiple pumps running.

Unsteady modulation at 0.12 Hz is also indicated in Figure 9. The modulation appears to gradually build up throughout three-pump operation and yet stays strong when the 0.01 Hz modulation drops in frequency, which suggests this modulation may not be associated with the PCPs.

Other virtual channels can be used to gather additional data. The virtual channels can provide corroborating information and data with a different perspective. Figure 10 shows the virtual channel for the second pump frequency at 298 Hz. This spectrogram looks surprisingly like Figure 9 but with a few intriguing differences. The spectrograms of higher order pump harmonics tend to have a lower signal to noise ratio than the first (fundamental) order pump harmonics. While the signal to noise ratio in Figure 10 is better than expected, it is still not as good as in Figure 9. It is surprising the second pump frequency has a much stronger second order modulation harmonic at 0.02 Hz than the first pump frequency.

The information provided by the first and recursive uses of the STFFT is sensitive to the rotational speed of the PCP shaft and the level of vibrational energy the pumps produce. When a single pump is running, the first use of STFFT is appropriate to use and baseline for health monitoring. Each pump has a characteristic operational frequency and vibration level that can be measured and tracked. The pumps can be baselined when first operational. A deviation from the baseline frequency or change in amplitude is either a variation in the wear of the pump or an operational change. Thus, by keeping track of operational changes the health of the pump can be determined or by running individual pumps under the same conditions prior to reactor start up. When multiple pumps are running with closely spaced frequencies, the pump frequencies interfere with each other, causing interference and frequency modulation of the pump's amplitude signals. Recursive application of the STFFT is used to provide useful information when several pumps are interfering. The resulting output tracks the frequency modulation created by the interference of the pumps as shown in Figure 11 for three-pump operation. For three-pump operation, the recursive spectrogram can get complicated. The STFFT is a very sensitive data processing technique that can provide better than 0.01 Hz resolutions and is able to detect subtle changes in the interactions between pumps and changes in the plant's operating conditions, as will be demonstrated in the next section. The next sections in this report will discuss more advanced data analysis techniques.

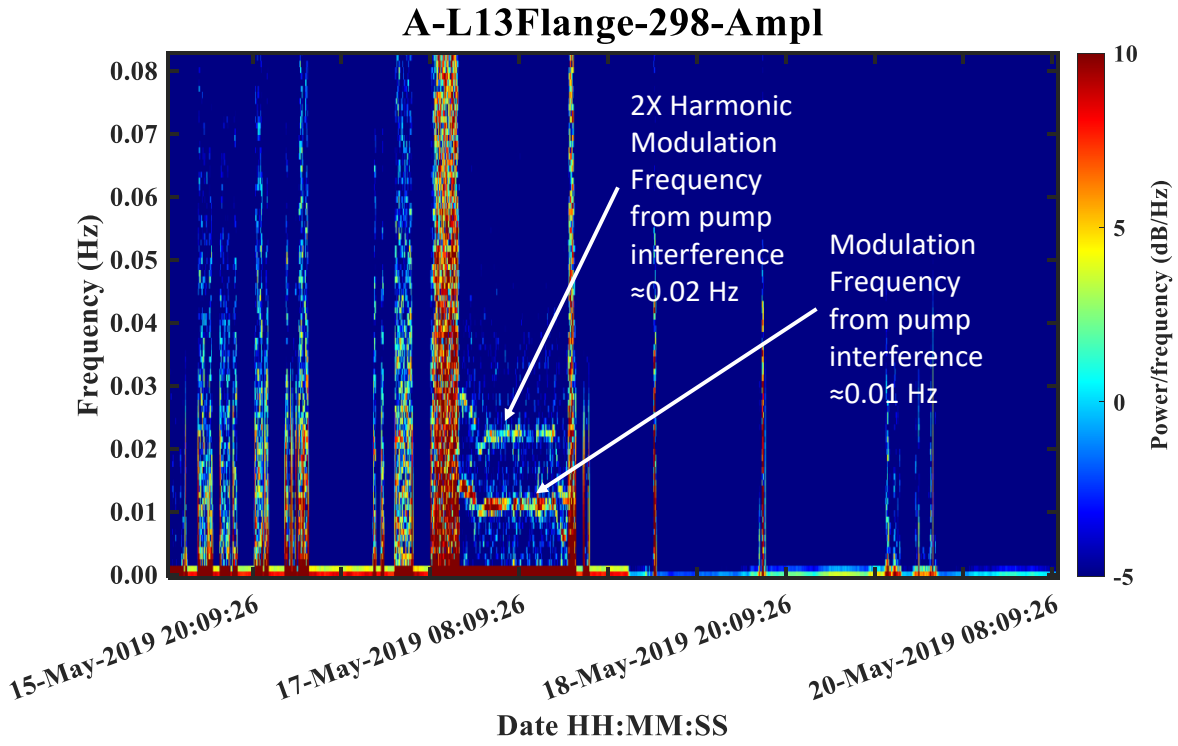

Figure 10. The second harmonic of the pump frequency can provide additional information. The higher harmonics of the pump frequency can provide higher fidelity but generally at the cost of lower signal to noise ratio.

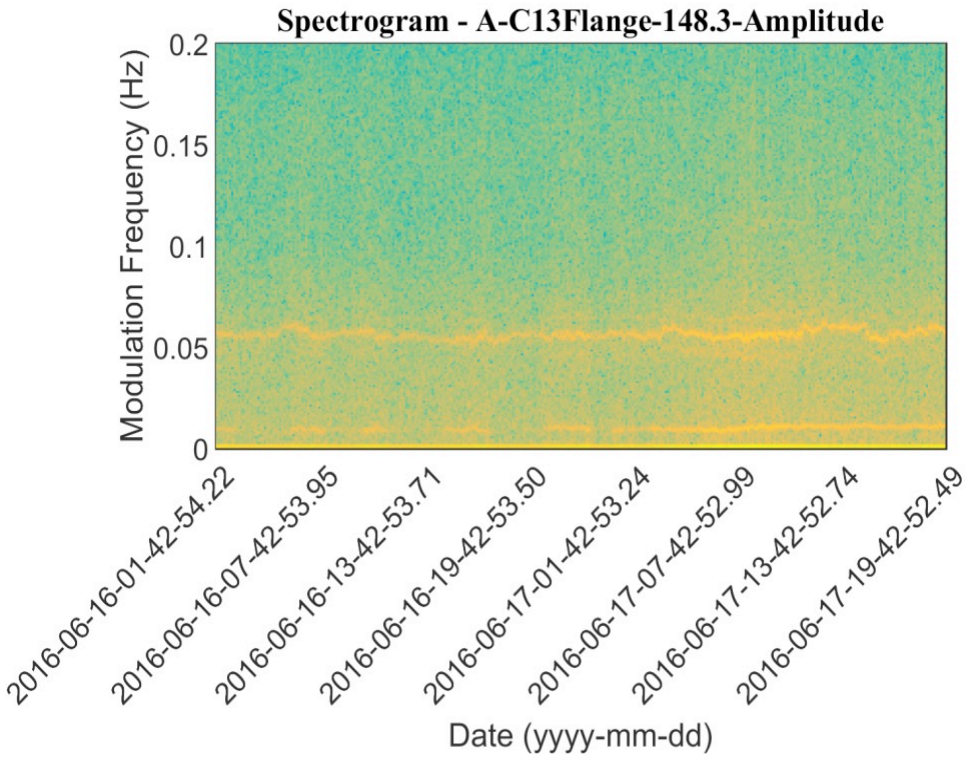

Figure 11. Three PCPs are running; there are two distinct modulation frequencies: 0.01 and 0.06 Hz. The upper and lower traces that are centered on the 0.06 Hz trace are caused by intermodulation from the other pumps. The intermodulation can be best seen in the 0.06 Hz trace near the end of the spectrogram.

4. ACOUSTIC SPECTROGRAMS

4.1 Primary Coolant Pumps Combinations

ATR has four PCPs to provide cooling fluid (i.e., water) during its operation. These four PCPs are divided into two sets. Set 1 includes the PCPs labeled M6 and M7, and Set 2 includes the PCPs labeled M8 and M9. ATR operations are categorized into normal operations and PALM cycles. During normal operations, two PCPs are operated, one from each set. Two PCPs from the same set are not operated to ensure structural health of the siting foundation of PCPs. During PALM cycles, three PCPs operate. The possible combinations of PCPs for normal and PALM cycles for which acoustic data have been logged are summarized in Table 2 and processed using the recursive STFFT approach. Note, that the PCP M9 is running for the PALM cycles. It should not be inferred that the PCP M9 is required for PALM cycle; rather the combinations M6, M7, and M8 is still a possibility.

Table 2. Possible combination of PCPs operation during normal and PALM cycle.

	Set 1		Set 2	
ATR Operation	M6	M7	M8	M9
Normal	On	Off	On	Off
	On	Off	Off	On
	Off	On	On	Off
	Off	On	Off	On
PALM	On	Off	On	On
	On	On	Off	On
	Off	On	On	On

4.2 Acoustic Spectrograms during Normal Operation

Spectrograms in Figure 12–Figure 15 represent the amplitude modulation caused by the interference between two-pump frequencies close to 148.3 Hz when two PCPs are running during normal ATR operations. From the spectrograms, the following observations are inferred:

1. The frequency modulation close to 148.3 Hz is consistent across all the PCP combinations, and it varies between 0.05Hz and 0.1Hz.
2. The spectrogram for each PCP combination is unique.
3. The spectrogram of PCP combinations, M6 and M8, and M7 and M8, comprise monostable and bistable states. The bistable state exhibits a cyclic amplitude modulation and tends to appear as the reactor is approaching criticality and as the reactor is prepared for shutdown. Here monostable state refers to a single and stable amplitude modulation when PCPs are operated. Bistable state refers to cyclic change in the amplitude modulation with stable periodicity when PCPs are operated.
4. The spectrogram for the M7 and M9 combination exhibits the bistable state during the steady-state operation of the ATR (see Figure 15).
5. The spectrogram for the M6 and M9 combination has bistable state for the entire reactor operation (see Figure 14).

These unique characteristics in the spectrogram are captured to develop acoustic signatures that are used to train machine learning models to automate the classification of ATR operation and identify PCP combinations. Figure 12–Figure 15 show the acoustic signature for different PCP combinations during normal operation for the data collected using the accelerometer at HSIS. Similar spectrograms are generated using the data from other sensor locations with slight variations in the intensity of the signal which could be due to signal attenuation through different paths within the transmission material.

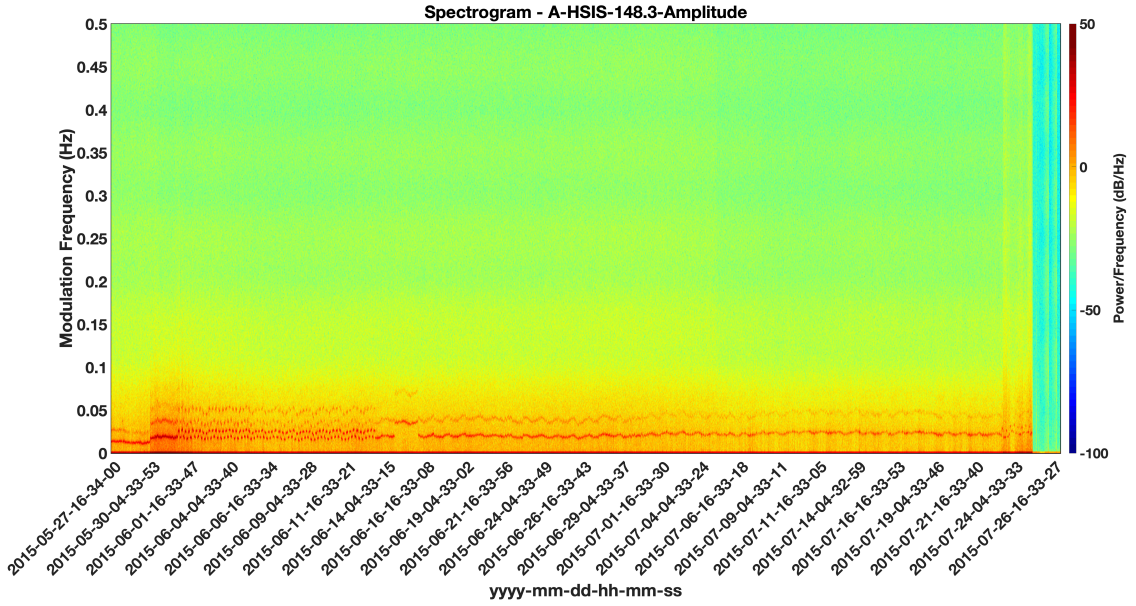
Spectrogram - A-HSIS-148.3-Amplitude
Modulation Frequency (Hz)
0.5
0.45
0.4
0.35
0.3
0.25
0.2
0.15
0.1
0.05
0
50
0
-50
-100
Power/Frequency (dB/Hz)
2015-05-27-16-34-00
2015-05-30-04-33-53
2015-06-01-16-33-47
2015-06-04-04-33-40
2015-06-06-16-33-34
2015-06-09-04-33-28
2015-06-11-16-33-21
2015-06-14-04-33-15
2015-06-16-16-33-08
2015-06-19-04-33-02
2015-06-21-16-33-56
2015-06-24-04-33-49
2015-06-26-16-33-43
2015-06-29-04-33-37
2015-07-01-16-33-30
2015-07-04-04-33-24
2015-07-06-16-33-18
2015-07-09-04-33-11
2015-07-11-16-33-05
2015-07-14-04-32-59
2015-07-16-16-33-53
2015-07-19-04-33-46
2015-07-21-16-33-40
2015-07-24-04-33-33
2015-07-26-16-33-27
yyyy-mm-dd-hh-mm-ss

(a)

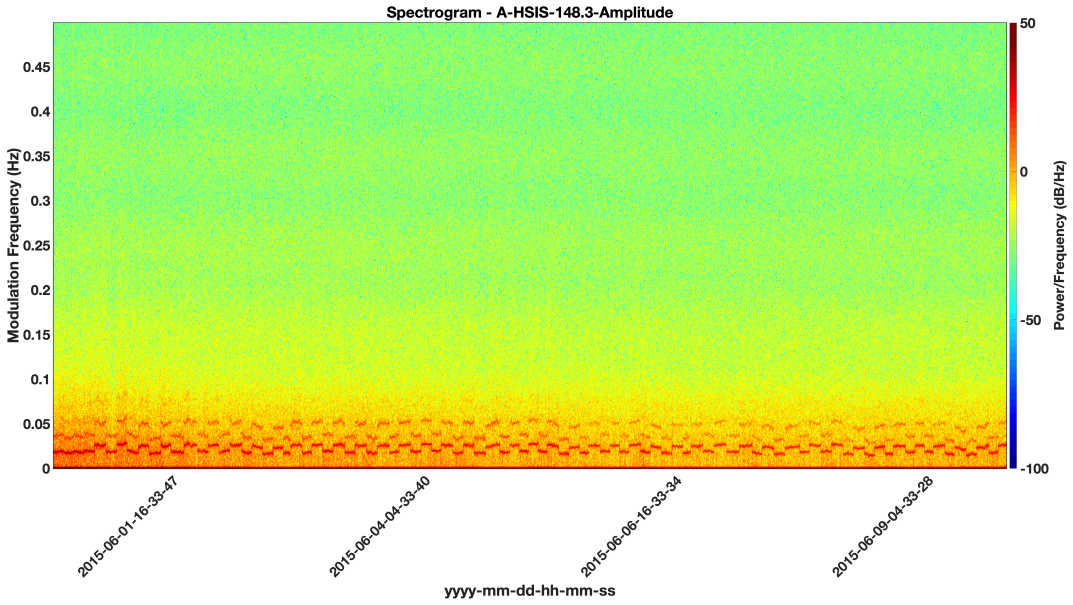
Spectrogram - A-HSIS-148.3-Amplitude
Modulation Frequency (Hz)
0.45
0.4
0.35
0.3
0.25
0.2
0.15
0.1
0.05
0
50
0
-50
-100
Power/Frequency (dB/Hz)
2015-06-01-16-33-47
2015-06-04-04-33-40
2015-06-06-16-33-34
2015-06-09-04-33-28
yyyy-mm-dd-hh-mm-ss

(b)

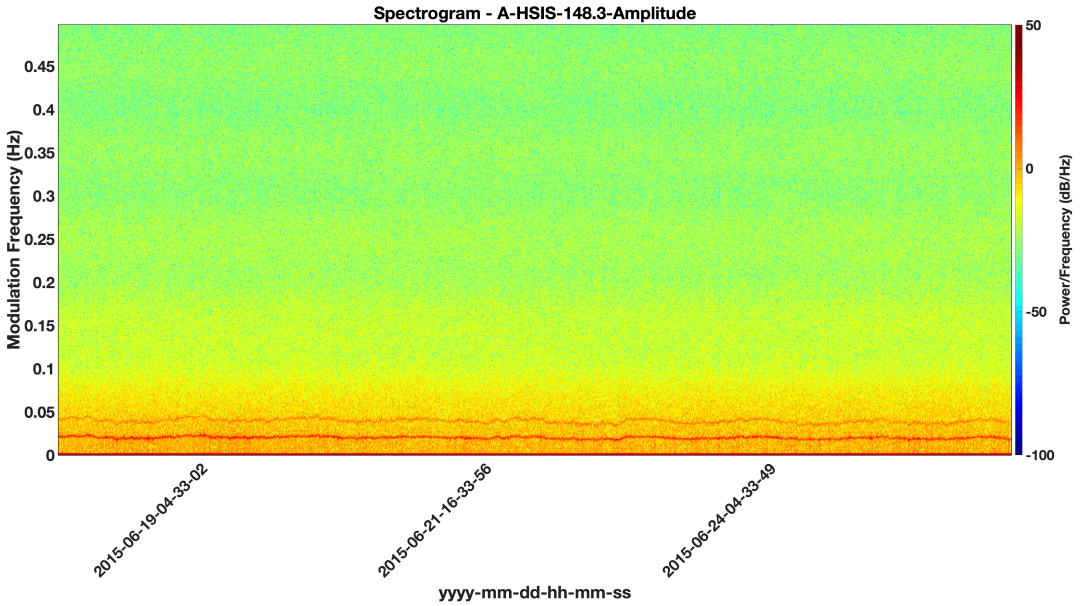

(c)

Figure 12. (a) Acoustic baseline signature of ATR collected during reactor operation for M6 and M8 combination using the AMI. (b) Bistable state observed during reactor operation. (c) Monostable state observed during reactor operation.

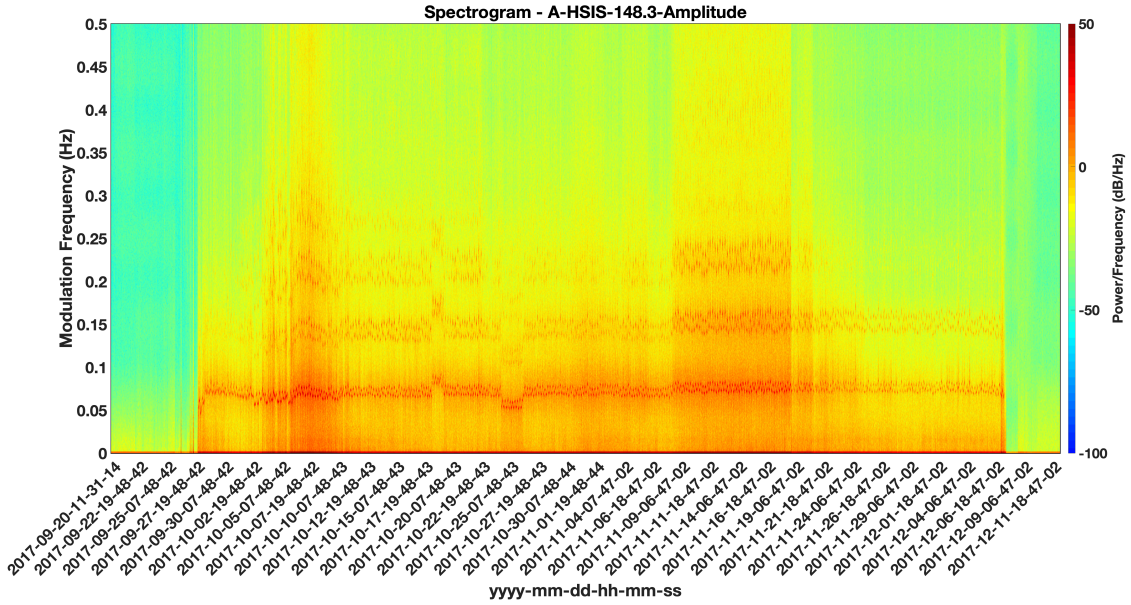

Figure 13. Acoustic baseline signature of ATR collected during reactor operation for M6 and M9 combination using the AMI.

Figure 14 captures ATR's normal operation with M7 and M8 PCPs running. During operation, two events are observed leading to reactor shut down for a short period before restarting. The first event is related to ATR switching operations to back-up diesel generators because the 480V commercial power source was taken out of service. This event causes a jump in the amplitude at modulating frequency around 148.3 Hz. This reflects how the modulating frequency of two pumps around 148.3 Hz is sensitive to the event and can be detected from the acoustic spectrogram. The second event is related to a seal break of the emergency pump leading to a reactor shutdown. The seal break is highlighted in the spectrogram (Figure 14b) with sharp rise in the intensity of the amplitude around 148.3 Hz modulation frequency.

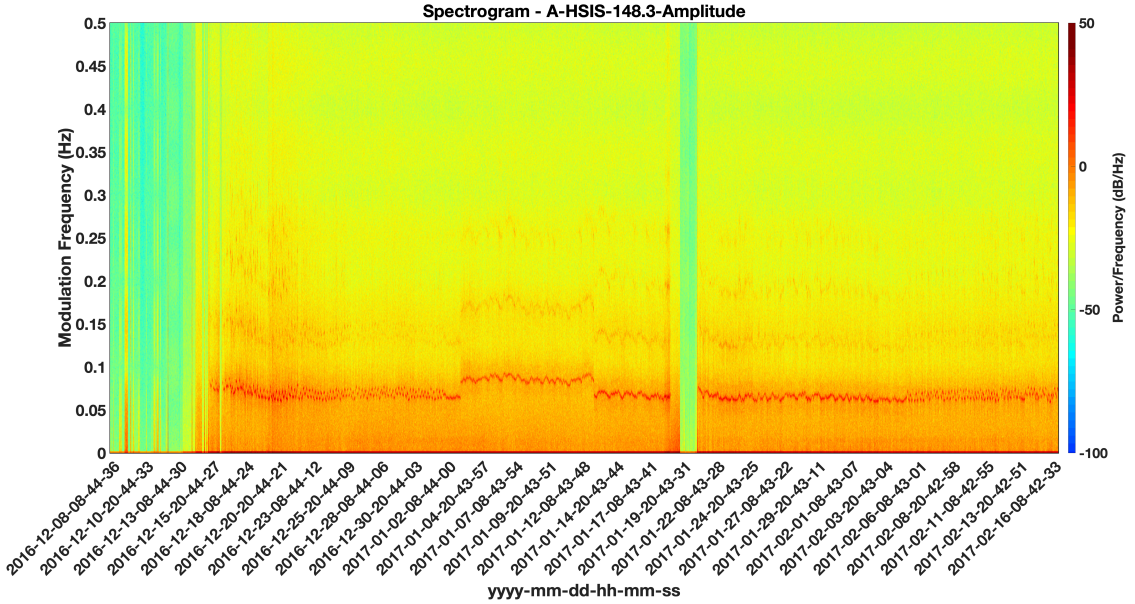

(a)

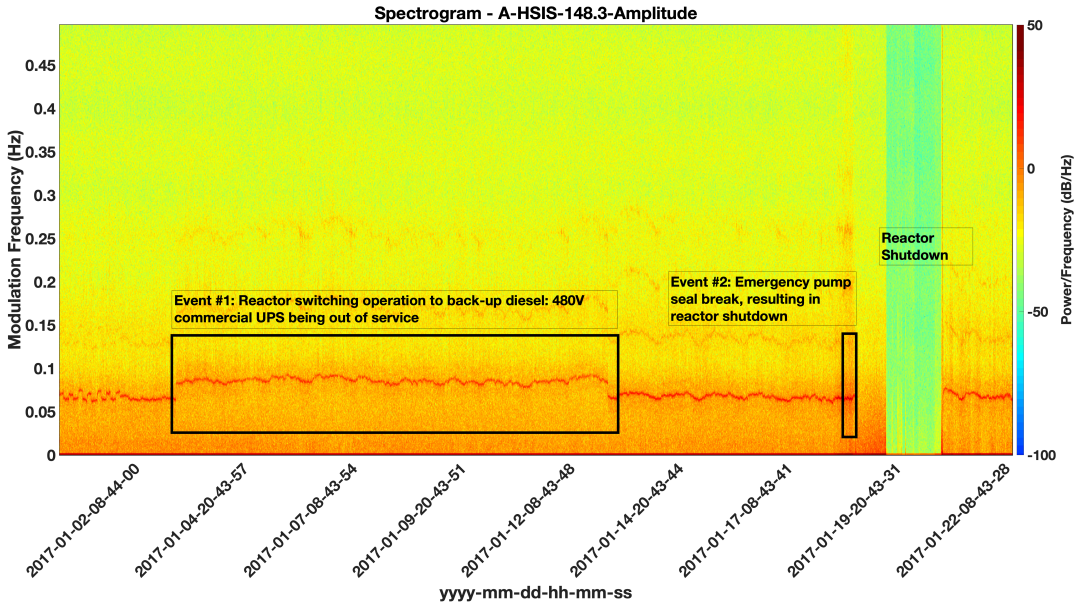

(b)

Figure 14. (a) Acoustic baseline signature of ATR collected during reactor operation for M7 and M8 combination using the AMI. (b) Two events highlighted were observed during reactor operation.

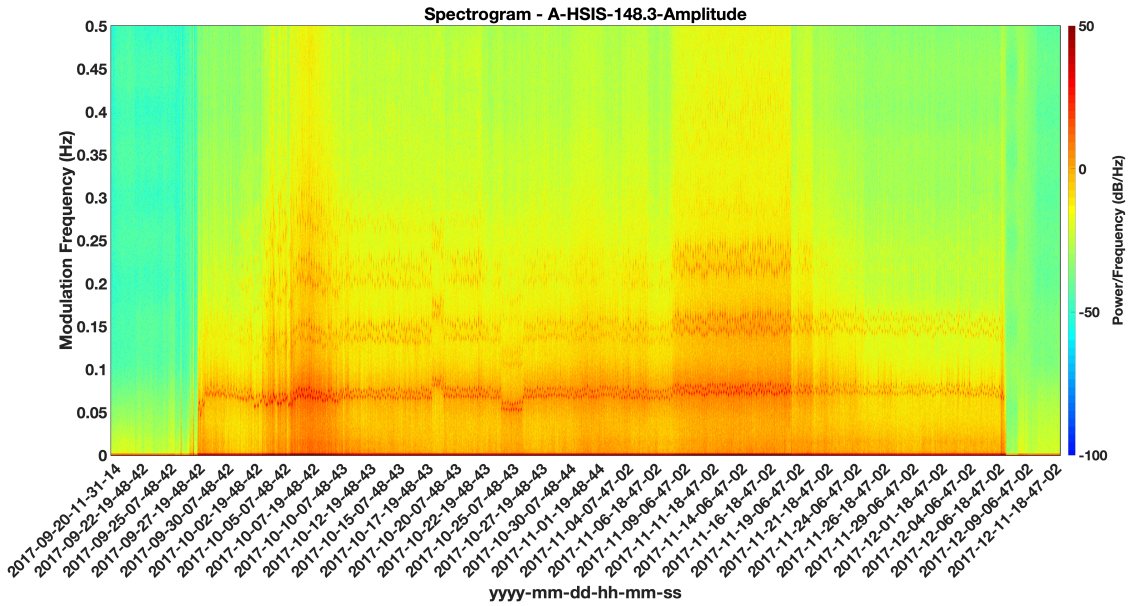

Figure 15. Acoustic baseline signature of ATR collected during reactor operation for M7 and M9 combination using the AMI.

4.3 Acoustic Spectrogram for Power Axial Locator Mechanism Cycle

ATR occasionally operates in a PALM cycle during which three PCPs are operated, and the reactor power changes from 50 to 200 MW. The duration of a PALM cycle is normally 14 to 21 days, significantly shorter than normal ATR cycles, which vary from 60 to 90 days. Figure 16–Figure 18 shows the acoustic signature generated for three PALM cycles for different PCP combinations at the L2 flange location. The acoustic signature shows the frequency modulation due to three PCP interferences close to 148.3 Hz. Compared to normal ATR acoustic signatures, PALM cycle signature exhibit two distinct modulations between 0 Hz and 0.01 Hz. These modulations also comprise of monostable and bistable states depending on PCP combinations. Specifically, the PALM cycle (Figure 17) for the PCP combination of M6, M7, and M9 exhibit cyclic bistable modulation compared to other PALM cycles that exhibit monostable modulation.

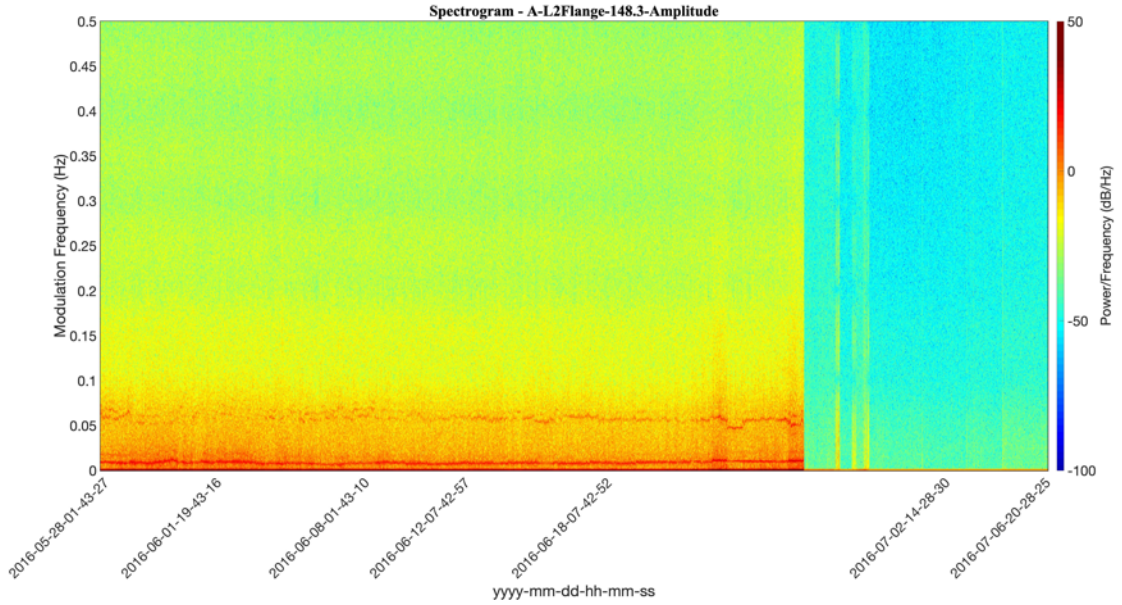

Figure 16. Acoustic baseline signature of ATR collected during PALM cycle for M6, M8, and M9 combination using the AMI.

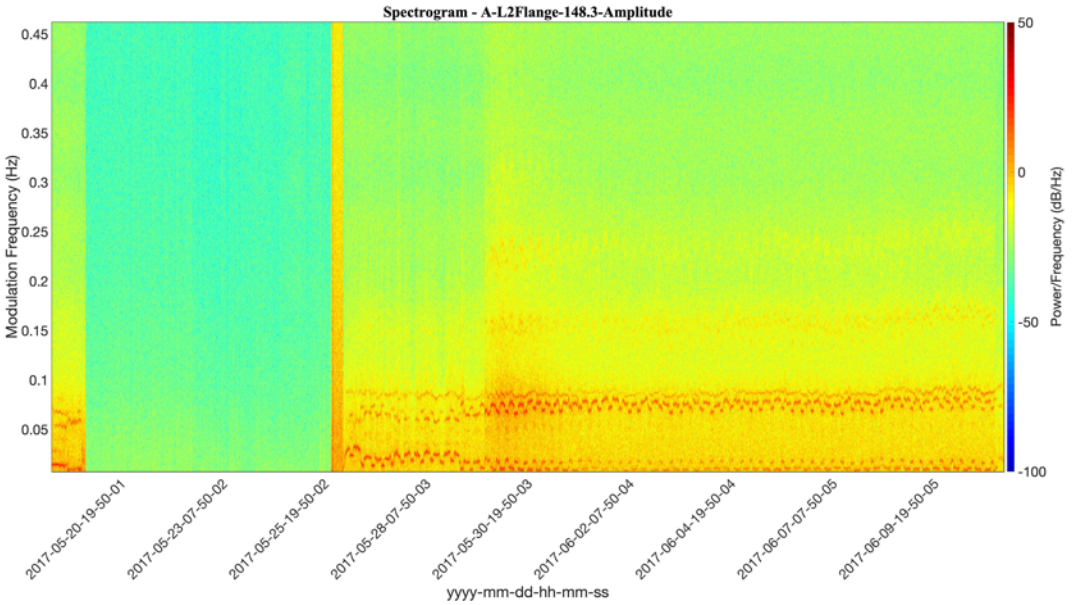

Figure 17. Acoustic baseline signature of ATR collected during PALM cycle for M6, M7, and M9 combination using the AMI.

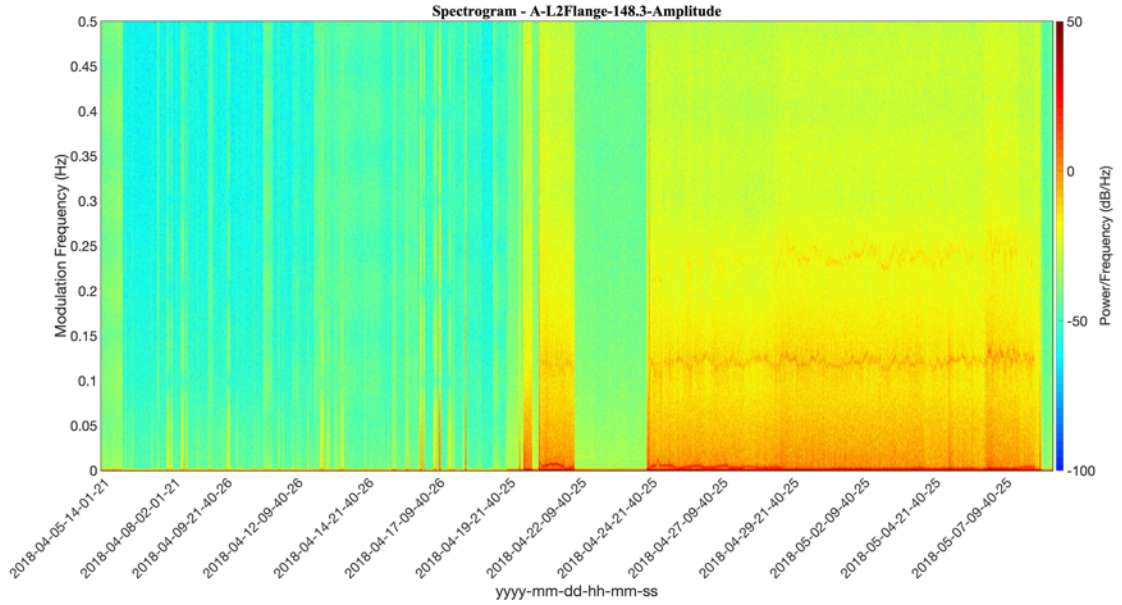

Figure 18. Acoustic baseline signature of ATR collected during PALM cycle for M7, M8, and M9 combination using the AMI.

During the 2016 PALM cycle, an event happened that signified two things. First, placing accelerometers at different locations within the ATR nozzle trench area enabled detection of the event. Second, using acoustic signatures, internal ATR structural health monitoring is feasible. Figure 9 shows the acoustic signature of the ATR PALM cycle at the L2 flange location. Figure 19 shows the signature of the ATR PALM cycle at the HSIS location. Comparing Figure 9 and Figure 19, totally different acoustic signatures are generated. At first, it was assumed the channel connecting HSIS accelerometer to the data acquisition system had failed. However, further investigation revealed a Beryllium block that was installed in 2004 and is connected to the HSIS internally had cracked, disturbing the HSIS signature.

Figure 20 shows the FFT generated using 2016 and 2017 PALM cycle data at HSIS and C13 flange locations. Observe, the FFT signal from 2016 has a spike around 5 kHz at both the locations and a spike at 9.8 kHz at HSIS location alone. Both spikes were due to cracking of the Beryllium block and are not present in the FFT of 2017 PALM cycle data for both the locations. This change in the FFT is due to removal of the cracked Beryllium block that was connected to the HSIS.

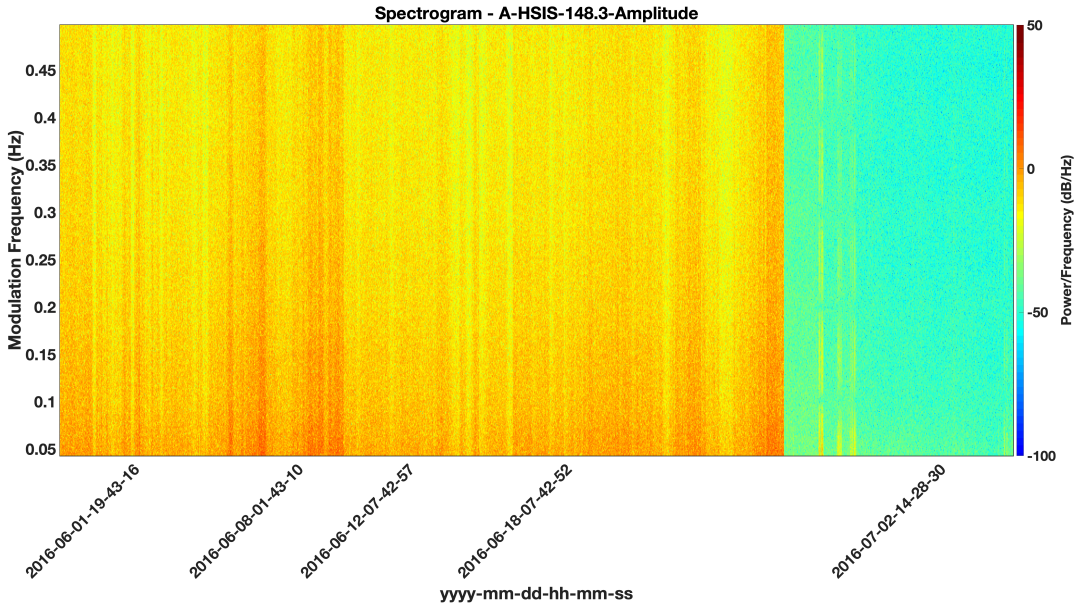

Figure 19. Acoustic baseline signature of ATR collected during PALM cycle for M7, M8, and M9 combination using the AMI at the HSIS location.

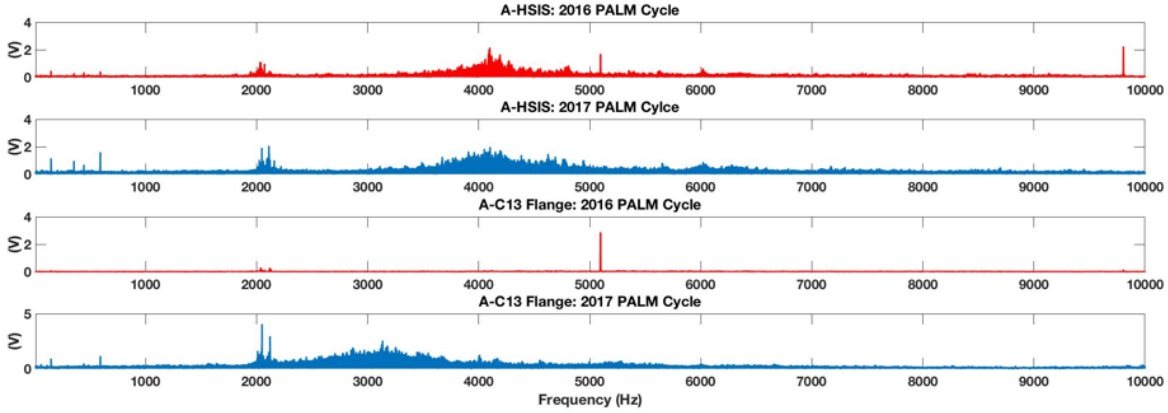

Figure 20. FFT plot of the ATR PALM cycles from 2016 and 2017 at HSIS and C13 flange locations.

5. PREDICTIVE MODELS

One of the goals of this project is to develop machine learning models capable of classifying the current operational state of the ATR based on acoustic signatures. In addition, the models should be able to diagnose the condition of the PCPs, and even reactor internals based on the features extracted from the acoustic data and acoustic signatures. In this report, two machine learning models are developed to automate the classification between different operational states during normal ATR operations based on the acoustic spectrogram. Two machine learning models, SVM and LDA, were developed to classify the events. A brief description on SVM and LDA is presented below.

5.1 Machine Learning Models

5.1.1 Support vector machines

SVM is an advanced pattern recognition and regression technique that attempts to address existing problems with the ill-posed nature of neural network (NN) training [29]. The goal of SVM training is to minimize the expected prediction risk on future data. In its most general setting, the problem of learning from the data can be formulated as follows [30]: given a data-generating mechanism, which is represented by a joint distribution $P(X,Y) = P(X)P\left(\frac{Y}{X}\right)$, where $X \in R^N$ and $Y \in R$ or {-1,1} depending on what problem we consider (regression or classification), $P(X)$ is a probability density function of input patterns or data, and $P\left(\frac{Y}{X}\right)$ is the probability of output conditioned on the input to find a function, $f_w(X)$, that would minimize the expected prediction risk on future data. In practice, instead of having probability distribution $P(X,Y)$, samples from input-output data distribution, referred as $D_n = (X_1, Y_1), \dots, (X_n, Y_n)$ are available. Given a set of parameterized functions $f_w(X)$, the goal is to find parameters w (weights) that minimize the discrepancy between Y and $f_w(X)$. This discrepancy is called a loss function and can be written as $L(Y, f_w(X))$.

A typical example of a loss function is the L_2 loss function, given by $L_2 = \left(Y - f_w(X)\right)^2$ or the squared distance between target Y and predicted value $f_w(X)$. The expected or true prediction risk is defined as a mathematical expectation of $L(Y, f_w(X))$ as:

$$R(w) = \int_{\{X,Y\}} L\big(Y, f_w(X)\big)P(X,Y)dXdY \quad (1)$$

Obviously, the true risk cannot be found in practice because the data-generating distribution $P(X,Y)$ is generally unknown, and what is available is only a sample of it (i.e., D_n). As a result, the minimization of true risk (Equation 1) in practice is replaced by the minimization of empirical risk, which is defined as:

$$R_{\{emp\}}(w) = \frac{1}{n}\sum_{\{i=1\}}^{n} L(Y_i, f_{w(X)}) \quad (2)$$

It can be shown [30] with infinite amounts of data, the function minimizes empirical risk also minimizes true risk [30]. However, empirical risk can be too optimistic when based on limited amounts of data, thus producing an overfitting learning machine. It can be shown [30] the true risk of misclassification is bounded from above by a sum of empirical risk (Equation 2) and VC-confidence where VC-confidence is a function of Vapnik–Chervonenkis (VC) dimension which measures "complexity" of a learning machine. The SVM is a machine learning method which classifies the data by minimizing empirical risk and VC dimension at the same time, thus producing classification boundaries with minimal true risk of misclassification. To achieve this, SVM projects the data into high-dimensional feature space where the data are likely to be linearly separable, and VC dimension can be estimated. The SVM's tunable parameters are kernel type, its parameters, if any, and regularization parameter which trades off misclassification rate and model's complexity are optimized using a cross-validation technique. As a result of data mapping to higher dimensional feature space, SVM always solves quadratic minimization problems, thus avoiding the problem of local minima.

In this report, nonlinear SVM with radial basis function kernel was used for classification. The kernel type was selected due to its ability to project the original data into infinite dimensional feature space, thus increasing chances of linear separability.

5.1.2 Linear discriminant analysis

Despite the proliferation of nonlinear classification techniques, many real-world data sets are separable with linear hyperplanes [31]. To validate this conjecture, LDA has been applied to the same data. LDA is a supervised classification technique closely related to principal component analysis which does not require class labels to best explain the data [32].

The LDA assumes Gaussian distribution for both classes and then uses Bayesian decision rule to assign the probability of each test pattern belonging to a specific class. The separating hyperplane is calculated based on statistical analysis of the training data, specifically mean values and covariance matrixes for different classes. The LDA assumes covariance matrix equality for the two classes. The LDA cost function is the ratio of between class variability to within-class variability, and it is maximized when the distance between the class means and the reciprocal of within-class variability are maximized. The obtained decision boundary is a hyperplane in the feature space.

5.2 Results

For this purpose, data from the 2016–2017 timeframe, for all the locations, were selected. The data for the PCP combination of M7 and M8 (Figure 14) is randomly divided into training and testing data using the 70-15-15 rule (i.e., 70%of the data is used for training, 15%for validation, and remaining 15% for testing). Class 1 corresponds to normal steady-state operation while Class 2 corresponds to any event that may be caused due to start up, shut down, or due to other actions. In this example problem, there were two main transients caused by events described in Section 4.2.

The selected data has a total data point number of 21,600. Out of 21,600, 15,120 data were selected for training, 3,240 data for validation, and 3,240 data for testing. The SVM kernel hyperparameters as well as regularization parameter have been optimized using cross-validation. The results of the classification using SVM and LDA models are presented in Table 3 and Table 4 respectively.

Table 3. Classification result using SVM model.

Test samples = 3,240	Predicted Class 1 (Normal)	Predicted Class 2 (Events)	Accuracy
Actual Class 1	1,600	20	0.9815
Actual Class 2	35	1,585	0.9782

Table 4. Classification result using LDA model.

Test samples = 3,240	Predicted Class 1 (Normal)	Predicted Class 2 (Events)	Accuracy
Actual Class 1	1,575	45	0.9720
Actual Class 2	50	1,570	0.9691

Initial results obtained by the application of SVM and LDA are encouraging. A similar approach can be applied to other acoustic spectrograms from other PCP combinations. An approach of data fusion is also a possibility for data from different PCP combinations during normal operation to build in robustness.

6. CONCLUSIONS

This report discussed developing a recursive STFFT approach to process acoustic signals when multiple pumps are running. The STFFT is derived from the repetitive application of the FFT, and the single use of the STFFT is appropriate to process acoustic signals generated by a single pump. The ATR brush data was analyzed using the recursive STFFT to understand the multiple pump interferences and to develop spectrograms for different primary coolant pump combinations. The STFFT is a very sensitive data processing technique that can provide less than 0.01 Hz resolutions and is able to detect subtle changes in the interactions between pumps and changes in the plant's operating conditions. The combination of PCPs for normal and PALM operations at ATR are unique and generate different signatures. These acoustic signatures were used to develop machine learning approaches to automatically

classify different operating regimes. This lays the foundation for a predictive analytic framework that can be leveraged by ATR to optimize their operations and maintenance.

The path forward involves continued engagement with ATR and expanded implementation of the AMI and predictive framework at ATR, other facilities within Idaho National Laboratory, and other experimental reactors, to prove the value of acoustic monitoring to inform the maintenance schedules of nuclear power plants and to enable a predictive maintenance model.

7. REFERENCES

1. Nuclear Science User Facilities. n.d. Homepage. https://nsuf.inl.gov. Last accessed on September 7, 2021.
2. Ali, R. A., S. L. Garrett, J. A. Smith, D. K. Kotter. 2013. "Thermoacoustic thermometry for nuclear reactor monitoring." IEEE J. Instrumentation & Measurement 16(3): 18–25. https://doi.org/10.1109/MIM.2013.6521130.
3. Garrett, S. L., J. A. Smith, R. W. M. Smith, B. J. Heidrich, M. D. Heibel. 2016. "Fission-Powered In-Core Thermoacoustic Sensor." Appl. Phys. Lett. 108: 144102. https://doi.org/10.1063/1.4944697.
4. Garrett, S. L., J. A. Smith, D. K. Kotter. 2013. Thermoacoustic Enhancements for Nuclear Fuel Rods. by. U.S. Patent 13/968,936, filed August 16, 2013, and issued February 20, 2014.
5. Fatemi, M. and J. F. Greenleaf. 1998. "Ultrasound-Stimulated Vibro-Acoustic Spectrography." Science 280 (5360): 82–85. https://doi.org/10.1126/science.280.5360.82.
6. Transient Reactor Test (TREAT) Facility. Transient Testing. Last accessed on September 7, 2021. https://transient.inl.gov/SitePages/Home.aspx.
7. Woolstenhulme, N. E. 2012. "AFIP-6 MKII First Cycle Report." INL/EXT-12-25170, Idaho National Laboratory.
8. PCB Piezotronics. n.d. "PCB Model 355B04." Products. Last accessed on September 7, 2021. http://www.pcb.com/products.aspx?m=355B04.
9. National Instruments. n.d. "NI 9205." Support. Last accessed on September 7, 2021. http://sine.ni.com/nips/cds/view/p/lang/en/nid/208800.
10. Smith, J. A., V. Agarwal, J. K. Jewell. 2017. Acoustic Measurement Infrastructure Method and System for Process Monitoring, Diagnostics and Prognostics. U.S. Patent 15/815,422 filed November 16, 2017 and issued May 17, 2018.
11. Smith, J. A., J. K. Jewell, J. E. Lee. 2015. "Flexible Data Acquisition Architecture For Novel Sensor Development and Deployment." Presented at Future of Instrumentation International Workshop 2015, National Rural Electric Cooperative Association Conference Center, Arlington, VA, May 4–6, 2015.
12. Agarwal, V., M. S. Tawfik, J. A. Smith. 2015. "Acoustic Emission Signal Processing Technique to Characterize Reactor In-Pile Phenomena." INL/CON-13-28878, Idaho National Laboratory.
13. Smith, J. A., S. L. Garrett, M. D. Heibel, V. Agarwal, B. J. Heidrich. 2016. "Progress In Developing An In-Pile Acoustically Telemetered Sensor Infrastructure." INL/CON-16-37719, Idaho National Laboratory.
14. Agarwal, V. J. A. Smith, J. K. Jewell. 2015. "Monitoring and Analysis of In-Pile Phenomena in Advanced Test Reactor using Acoustic Telemetry." INL/CON-14-32991, Idaho National Laboratory.
15. Smith, James A., Kotter, Dale K., Ali, Randall A., Garrett, Steven L., "Devices Synergistic With In-pile Nuclear Applications," Power Generation & Distribution Equipment Online Conference & Trade Show, GlobalSpec, Inc, September 11, 2013. INL/CON-13-28498, Idaho National Laboratory.

16. Agarwal, V., J. A. Smith. 2017. “Real-Time In-Pile Acoustic Measurement Infrastructure at the Advanced Test Reactor.” Nuclear Technology 197(3). https://doi.org/10.1080/00295450.2016.1273704.
17. Agarwal, V., J. A. Smith. 2017. “Assessing Advanced Test Reactor Process States Using Acoustic Measurement Infrastructure.” Presented at 2017 ASME Pressure Vessels & Piping Conference, Waikoloa, Hawaii, July 16–20, 2017. https://doi.org/10.1115/PVP2017-65474.
18. Smith, J. A., V. Agarwal. 2019. “Acoustic Measurement Infrastructure To Characterize Nuclear Reactor Operation." INL/CON-18-45089, Idaho National Laboratory.
19. Smith, J. A., V. Agarwal. 2019. “Taking Advantage of Intrinsic Processes For Process Monitoring, Diagnostics And Prognostics.”11th International Conference On Nuclear Plant Instrumentation, Control & Human–Machine Interface Technologies (NPIC & HMIT 2019), Renaissance Orlando At SeaWorld, Orlando FL, February 9–14, 2019.
20. Garrett, Steven L., Smith, James A., Smith, Robert W., Heidrich, Brenden J., Heibel, Michael D., “Using the Sound of Nuclear Energy,” American Nuclear Society’s Nuclear Technology, Vol. 195, No. 3, PP. 353-362, September 2016.
21. Agarwal, V., J. A. Smith, K. J. Jewell. 2015. “Monitoring and Analysis of In-Pile Phenomena in Advanced Test Reactor using Acoustic Telemetry.” INL/CON-14-32991, Idaho National Laboratory.
22. Hrisko, J., S. L. Garrett, W. M. Smith, J. A. Smith, V. Agarwal. 2015. “The Vibroacoustical Environment in a Nuclear Reactor.” Presented at Acoustical Society of America 169th Meeting, Pittsburgh, Pennsylvania, May 18–22, 2015.
23. Smith, J. A., B. J. Heidrich, V. Agarwal, M. D. Heibel, S. L. Garrett. 2016. “Using the Sounds of Nuclear Power.” Presented at 171st Meeting of the Acoustical Society of America, Salt Lake UT, May 23–27, 2016.
24. Agarwal, V., J. A. Smith. 2016. “Acoustic Telemetry Infrastructure for In-Pile ATR Monitoring.” Presented at ASME International Mechanical Engineering Congress & Exposition, American Society of Mechanical Engineers, Phoenix, AZ, Nov 11–16, 2016.
25. Agarwal, V., J. A. Smith. 2017. “Acoustic Measurement Infrastructure To Enable The Enhancement of Nuclear Reactor Efficiency and Safety.” Presented at Acoustics ‘17 Boston, the 3rd Joint Meeting of the Acoustical Society of America and the European Acoustics Association, Boston MA, June 25–29, 2017.
26. Smith, J. A., V. Agarwal. 2016. “Acoustic Measurement Infrastructure For Acoustic Sensor Telemetry.” Presented at Future of Instrumentation International Workshop 2016, National Rural Electric Cooperative Association Conference Center, Arlington, VA, May 2–4, 2016.
27. Smith, J. A., S. L. Garrett, M. D. Heibel, V. Agarwal. 2016. “Wireless In-Core Acoustic Telemetry and Self-Powered Sensing.” Nuclear Energy Enabling Technologies Crosscutting Technology Development (NEET CTD) Advanced Sensors and Instrumentation (ASI) newsletter, March 2016. Last accessed September 8, 2021. https://www.energy.gov/ne/downloads/advanced-sensors-and-instrumentation-newsletter-issue-4.
28. Allen, J. B. 1977. “Short Time Spectral Analysis, Synthesis, and Modification by Discrete Fourier Transform.” IEEE Transactions on Acoustics, Speech, and Signal Processing. ASSP-25 (3): 235–238.
29. Vapnik, V. 1995. *The Nature of Statistical Learning Theory*. New York: Springer-Verlag.
30. Vapnik, V. 1998. *Statistical Learning Theory*. New York: Wiley.

31. Fernández-Delgado, M., E. Cernadas, S. Barro, D. Amorim. 2014. “Do we Need Hundreds of Classifiers to Solve Real World Classification Problems?” Journal of Machine Learning Research 15 (90) 3133–3181.

32. Duda, R. O, P. E. Hart, and D. G. Stork. 2001. *Pattern Classification*. New York: Wiley.